8-4-2023

Discovering The Kinetic Behaviors Of Zeolites Of Mordenite, Ferrierite, Faujasite, Beta

Weixuan Huang
Syracuse University

Abstract

Fossil fuels have played a significant role in the development of nations. However, they have also given rise to various societal problems. In this context, Gamma-Valerolactone (GVL) emerges as a potential solution as a fuel additive and feedstock for the production of gasoline, jet fuel, and other products. GVL can undergo decarboxylation reactions facilitated by zeolite catalysts. Surprisingly, it has been observed that reactions taking place on different zeolites, despite having similar Brønsted acid site densities, exhibit distinct simulated initial rates. This research aims to compare the initial rate trends of mordenite and its poisoned derivatives with those of the MFI family, and provide explanations for the underlying factors causing these differences. Moreover, the same methodology will be applied to investigate zeolites such as Ferrierite, Fajusite, and Beta.

Discovering the Kinetic Behaviors of Zeolites of Mordenite, Ferrierite, Faujasite, Beta

By

Weixuan Huang

B.S., Edinburgh University / Liaoning Shihua University , 2017

Thesis

Submitted in partial fulfillment of the requirements for the degree of

Master of Science in Chemical Engineering.

Syracuse University

June 2023

Table of Contents:

1. Introduction

1.1 Background Information

The utilization of fossil fuels plays a crucial role in a country's economic growth [9]. However, the scarcity of fossil fuels, their inefficient use, and the resulting issues of excessive greenhouse gas emissions, particularly CO_2 production, have become pressing challenges for modern society [9]. These issues, including delayed development, global warming, and conflicts, highlight the urgent need for transition from traditional energy sources to renewable alternatives [1] [9].

First-generation biofuels, such as corn ethanol and biodiesel, have made significant contributions to reducing the reliance on fossil fuels [6]. However, Gamma-Valerolactone (GVL) presents an even more promising solution, as it can serve as an energy source and a precursor for various commercial products [12] [13] [14], including methyl tetrahydrofuran, levulinate esters, valeric esters, gasoline, jet fuel, and diesel [5]. Furthermore, GVL exhibits comparable performance to ethanol as a gasoline additive [12]. The primary feedstock for GVL production is levulinic acid (LA), which can be obtained from agricultural waste at a relatively low cost, with LA production rates exceeding 95% [3] [2]. The production processes for both LA and GVL are environmentally friendly and economically viable.

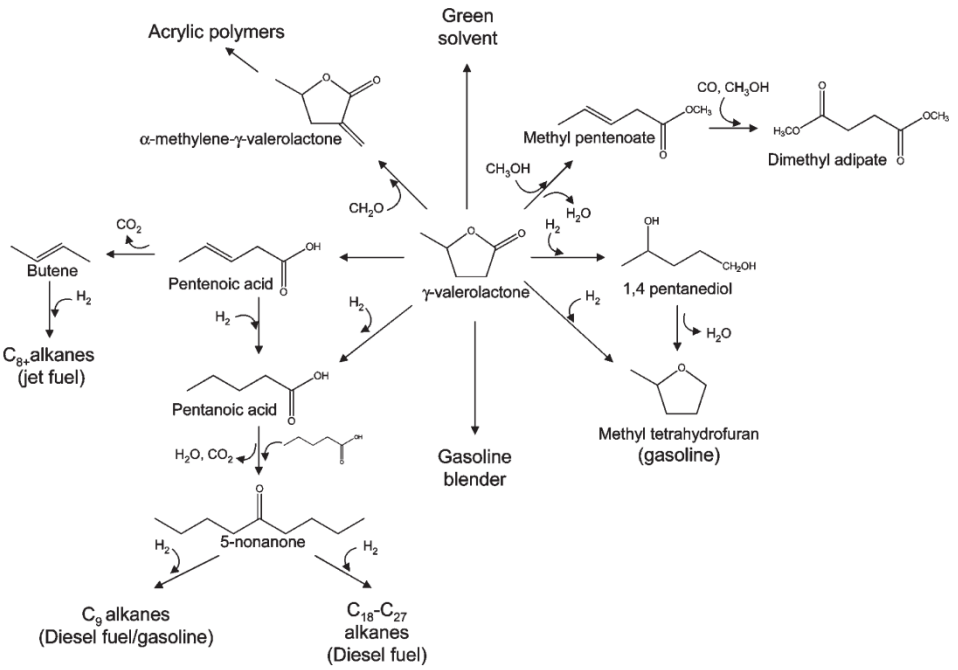

Figure 1 usage of GVL and its derivatives [9]

In the presence of acidic catalysts (Brønsted and Lewis sites), GVL undergoes ring-opening reactions, leading to the formation of chain-like structures with carbenium ions [11] [15]. Subsequently, the intermediates undergo decarboxylation, wherein the carboxyl group (-COOH) is eliminated, generating carbon dioxide, and the remaining group forming butene [11] [15]. Both butene and the resulting pentenoic acid (PEA) have great potential for further conversions into various chemical products. PEA can be used for alkane fuels, nylon precursors, 5-nonanone, valeric esters, and nylon production, while butene can serve as a substitute for aviation fuel through oligomerization processes [11].

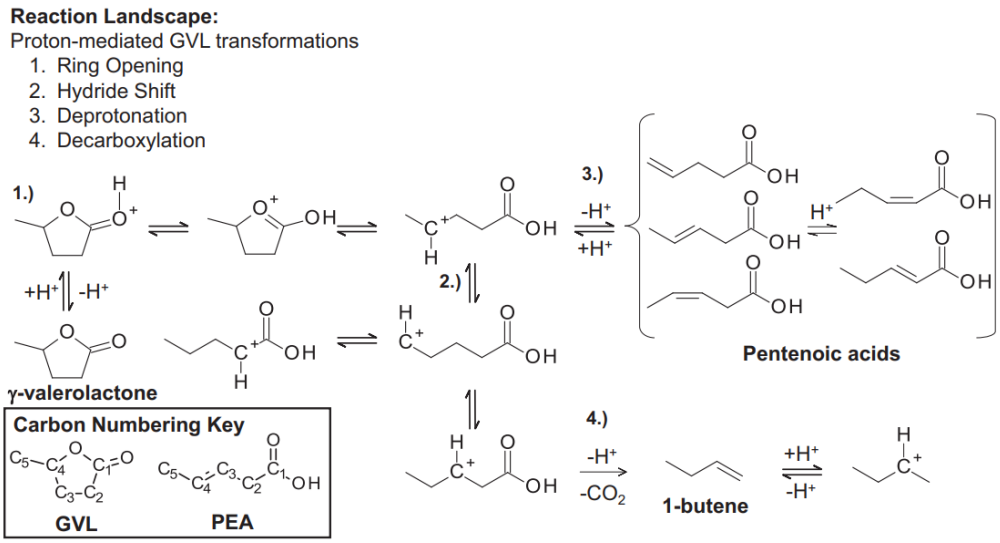

Figure 2 Decarboxylation process of GVL [11]

Zeolites are aluminosilicate minerals with diverse pore structures and varying compositions of silica and alumina [16]. Examples include mordenite, heulandite, and the MFI family of zeolites [16]. Zeolites are often regarded as Brønsted acid catalysts, in contrast to amorphous silica-alumina, which considers both Lewis and Brønsted acid sites effective [3].

1.2 Objective

The catalytic acid site density is positively correlated with the ability to catalyze chemical reactions. Previous studies have shown that the decarboxylation (DC) rate of MOR zeolite, though having the same Brønsted acid site density as MFI 23:1, was ten times lower than that of MFI 23:1 [4]. Similarly, FAU zeolite, despite having a larger surface area and pore area than MFI 30:1 and a similar site density, also exhibited a DC rate ten times lower than MFI [4]. Another comparison between MFI 80:1 and FER zeolite revealed a significantly lower DC rate for FER whose site density was twice as large as that of MFI 80:1 [4].

The differences in rate patterns might be attributed to variations in the physical structure o between MFI and MOR zeolites. In this study, we aim to investigate the initial rate development with respect to density by using the Koros and Nowark criterion under different temperature conditions. Additionally, Brønsted acid site density of mordenite was changed by poisoning effect using sodium nitrite solutions of various concentrations. Structural information as well as the reaction mechanism over the catalysts were applied to provide an explanation for the observed rate differences. Furthermore, the same analysis procedure will be applied to Ferrierite (FER), Faujasite (FAU), and Beta (BEA) zeolites.

2. Materials and Methods

2.1 Materials and Equipment

γ-valerolactone (GVL, >98%, Aldrich), trans-2-pentenoic acid (t2-PEA, Acros, 97%), MFI structure zeolite samples of different aluminium contents, Mordenite structure zeolite, Ferrierite, Faujasite, Beta, Isopropyl amine (IPA), Helium

silica chips (850-2000 um, 99.9%, Sigma Aldrich), gas chromatographer (HP-7890), type K thermocouple (Omega), temperature controller (Love, series 16A), mass-selective residual gas detector (Stanford Instruments RGA 100)

2.2 Catalyst Preparation and Storage

All catalysts used in this study were obtained from commercial suppliers. Prior to storage, the catalysts underwent a calcination procedure. In this procedure, the catalysts were placed at the center of a straight quartz tube with two pieces of quartz wool attached on both sides, and supported by silica chips (850-2000 μm, 99.9%, Sigma Aldrich) in lower dead volume. The catalysts could also be placed in a U-shaped tube configuration with the same method as

alternative. The tube was subjected to a continuous flow of air at a rate of 50 ml/min, and a temperature controller (Love, series 16A) was used to maintain the temperature at 450°C for a duration of 4 hours. The temperature ramping speed was set at 3°C per minute to prevent rapid evaporation of water molecules inside the catalysts. After calcination, the catalyst samples were carefully transferred to glass vials and covered with plastic film to prevent absorption of water vapor from the laboratory environment.

2.3 Zeolite Poisoning

Three groups of MOR catalysts, each weighted approximately 4 grams, were individually immersed in sodium nitrite solutions of different concentrations (0.01M, 0.1M, and 1M) at the temperature of 80°C for 12 hours. After the soaking process, the catalysts were subjected to vacuum filtration, followed by washing with 1 liter of deionized water. Subsequently, the catalysts were dried undergoing an overnight drying process in an oven at 90°C. Once dried, the catalysts were ground to a powder form and then subjected to calcination to obtain the powdered catalysts for further analysis.

2.4 Zeolite Brønsted Acid Site Density Determination

A quartz tube with a diameter of 1/2 inch was loaded with approximately 0.1g of the poisoned MOR catalyst. The catalyst was placed between two pieces of quartz wool and supported from the bottom by quartz chips. To determine the precise weight of the catalyst, the empty tube with chips, wool, and those loaded with the catalyst were separately weighed. The difference between the weighting was the precise weight of the catalyst loaded. The quartz tube was then wrapped with a heating tape and insulated with multiple layers of quartz wool. A temperature controller (Love, series 16A) was used to set and control the temperature.

After the calcination process, the catalyst was purified and cooled down for 90 minutes by helium gas flowed at a rate of 100 ml/min. The helium flow rate was then adjusted to 50 ml/min, and isopropyl amine (IPA) was injected into the gas stream to capture the catalyst surface. This process took approximately one hour.

For IPA desorption, the helium flow rate was increased to 400 ml/min for one hour to remove physically absorbed molecules. Helium containing 1% argon was later used for temperature programmed desorption (TPD), during which chemically adsorbed IPA reacted over the Brønsted sites, generating propene and ammonia.

Under steady flow conditions, the temperature controller increased the temperature of the reactor (quartz tube) at a rate of 5°C/min until reaching 500°C. A mass-selective residual gas detector (Stanford Instruments RGA 100) was utilized to monitor the signals of helium, argon, IPA, propene, and ammonia at the effluent. Since the stoichiometry values for the IPA catalytic reaction were all one, the cumulative amount of propene (in moles) detected by the RGA during the TPD process reflected the number of Brønsted sites on the catalyst surface.

2.5 Catalyst Deactivation Detection

Figure 3 illustrated the configuration of the catalyst deactivation system, which consisted of two streams: the bypass stream used for vaporizer and reactor calcination, and the experiment stream for GVL and PEA decarboxylation over MFI and MOR zeolites.

During the bypass stage, mass flow controller 8 (Brooks, model 5850S) delivered the air flow through the vaporizer, and it later entered the waste stream. The temperature ramping rate and calcination temperature for the air flow in the vaporizer were the same as discussed in Section 2.2. Reactor calcination, also known as catalyst regeneration, involved the removal of coke deposition over the active sites. Additional air flow entered Valve 1 at pore positions 5, and exited at 6 to flow into the packed bed. The temperature adjustment was the same as described in Section 2.2.

During the experiments, helium was used as the carrier gas and was delivered by mass flow controller 7. It entered Valve 1 at positions 1, and left at 6, flowing into the up-flow packed bed reactor, which was insulated in an aluminum furnace. The flow was then directed to the gas chromatograph (GC) (Agilent Technologies, GC 7890A) at Valve 3 for quantification analysis. The helium flow rate was controlled at 25 ml/min. Liquid GVL/PEA loaded in a syringe pump (Cole-Parmer, model 110) was preheated before entering the vaporizer and mixed with helium. The temperature of the vaporizer, reactor, and the rest of the tubing in the system was adjusted using variacs and PID controllers (Love, series 16A) with type K thermocouples. The temperature of the vaporizer and tubing was maintained between 150°C and 170°C.

The gas mixture initially passed through the bypass (directed to the GC) to ensure thorough mixing of GVL/PEA with helium. The GC area of GVL/PEA was recorded to ensure constant values. Afterwards, the flow was switched to the reactor at Valve 1, and the time at this moment was recorded as zero time on stream, indicating the first contact of the catalyst with the reactants.

For the packed bed specifications, catalysts were loaded into a 1/2 inch-diameter 316 stainless steel tube, with two pieces of quartz wool attached on both sides. The lower dead volume was filled with silica chips.

In data processing, GC areas were converted into molar flow rates per unit mass based on calibration relationships. The flow rate data was then plotted on a mass normalized reaction rate (μmol/g/min) versus time (hr) coordinate system, from which the initial flow rate was simulated.

As this research involved simulated initial rates for 15 different zeolites, the raw data (GC area) of GVL decarboxylation over MFI 23:1, 30:1, 50:1, 80:1, 200:1, 500:1, and PEA reaction over MFI 30:1, 80:1, 200:1, 500:1 was obtained from experiments conducted by Xinlei Huang.

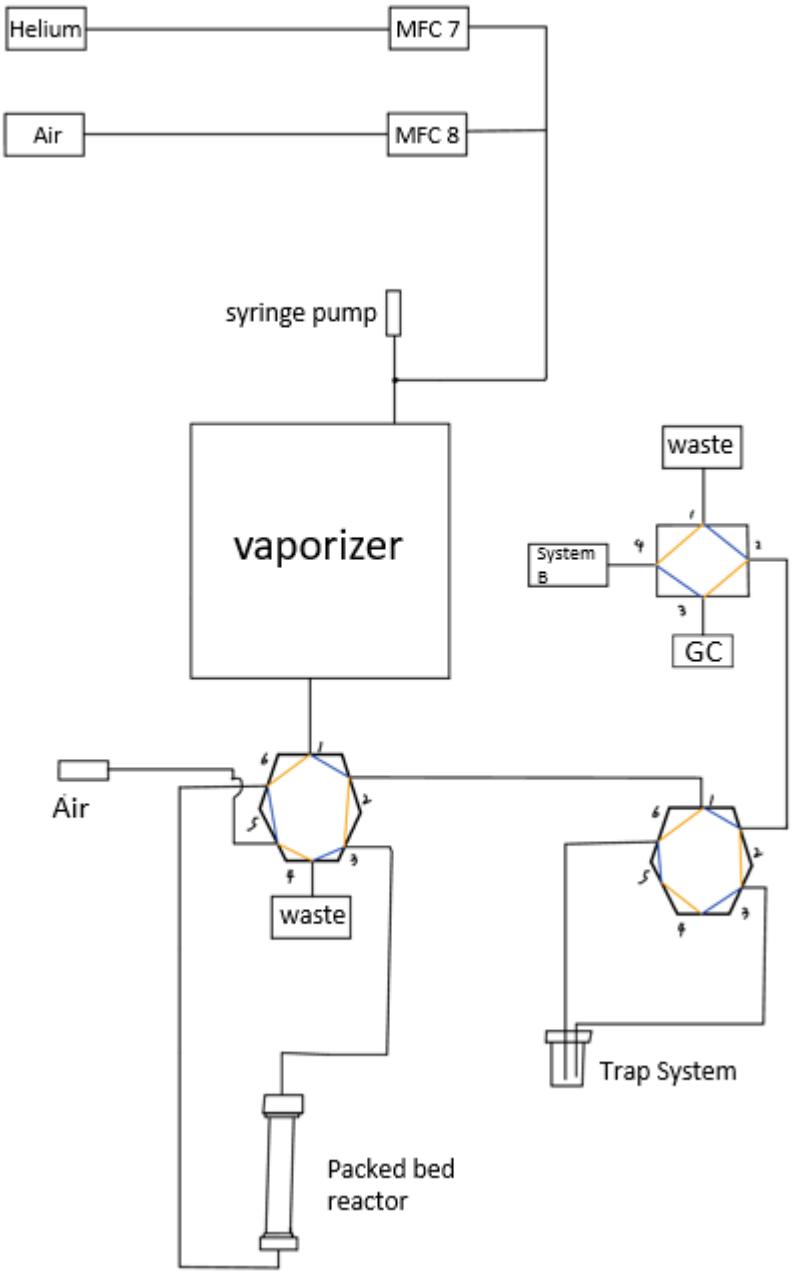

Figure 3 Decarboxylation system layout

3. Results and Discussions

3.1 Simulation Method Selection

This project aims to investigate the relationship between catalyst decarboxylation rate and catalyst active site densities of MFI, MOR, FER, FAU, BEA, and their poisoned derivatives, and explain the reasons causing the lower reaction rates of MOR, FER, FAU and BEA.

Catalyst deactivation plays a crucial role in the progress of reactions. During catalytic reactions, the active sites on the catalyst surface can undergo deactivation processes, including restructuring (sintering) or the accumulation of poisons, coke, or inert species [20].

In the case of sintering, catalyst particles can bond or fuse together, leading to the formation of larger particles and a reduction in the surface area and the number of active sites. This reduction in active sites impaired the production rate of the reaction [23]. In the accumulation scenario, the inhibitors can permanently or temporarily disable the active sites, leading to a decrease in the production rate [23].

In the current research, during reactions of decarboxylation, coke formation occurs on the catalyst surface due to the high reaction temperatures. This coke formation can lead to a decline in the rate of product formation (butene) over time (Figure 4). The decay in the rate follows a curve, with a rapid decrease in the early stages and a later gradual reduction.

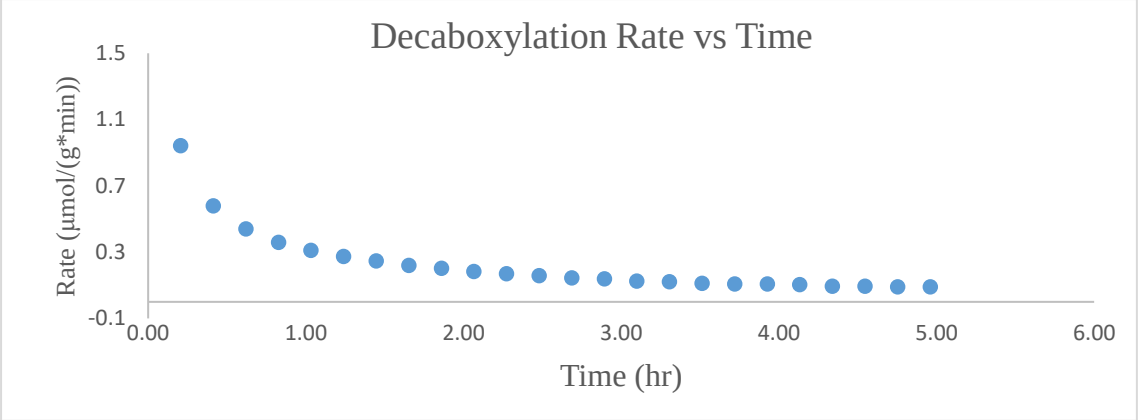

Figure 4 Butene Decaboxylation Rate vs Time over MFI 23:1 at 198°C using PEA as reactant

In the context of catalyst deactivation, comparing the reaction rates of different catalysts became challenging. However, when catalysts were initially exposed to the reactants at zero time on stream (explained in section2.5), deactivations had not occurred over the active sites. Therefore, the production rate observed at that moment, known as the initial rate, could eliminate the influence of catalyst deactivation and serve as a reliable reference for evaluating a catalyst's impact on the reaction. Previous studies indicated that Brønsted acid sites on zeolites could be restored to a fresh condition through calcination [4].

Nevertheless, obtaining direct measurements of initial rates was difficult due to various factors such as the design of the reaction system and diffusion processes within the reactor. Typically, data points for reaction rates were acquired during the deactivation process. One might have intuitively attempted to connect all the data points and extrapolate to zero time on stream. However, using straight lines to connect the data points was considered inappropriate since the intersection on the rate axis by extrapolation solely relied on the positional relationship between the first two data points, which failed to represent the overall data trend. Employing a hand-drawn curve that included as many data points as possible might be a better approach. However, this method had two major drawbacks: it became challenging to quantitatively assess the proximity of

each data point to the curve, and the hand-drawn extrapolation curves might fail to account for other influential factors such as the ring opening and closure reactions between GVL and PEA.

To identify a curve that adequately represented all the data points, one should have considered the application of the error sum of squares (SSE) function stored in the Solver in Microsoft Excel (Eq.1). This approach helped finding the best-fit curve that minimized the overall error between the curve and the data points, so it could provide a more accurate representation of the relationship between catalyst decarboxylation rate and catalyst active site densities.

$$SSE = \sum_{i=0}^{n}(measurement_i - model_i)\text{^}2 \quad \text{(Eq.1)}$$

SSE, the sum of squares of residuals, calculated the squared differences between experimentally obtained rates of reaction ($measurement_i$) and simulated rates of reaction ($model_i$) over a certain time scale. It represented the positional difference between the experimental data points and the simulated data points. A lower SSE indicated that the simulated data closely matched the measured ones. To generate a simulated reaction rate, a mathematical objective function was required to describe all the modeled points. By adjusting the parameters of the objective function, the Solver determined the function that minimized SSE, allowing the experimental data points to align with the simulated curve.

A polynomial function could be used as the objective function since it had a precise mathematical expression with adjustable parameters. However, polynomial functions exhibited a wave-like shape. While higher-order polynomial functions could include all the data points on the curve, they also introduced more waves, making the extrapolated parts less representative of the rate decay [22].

$$r = (R_0 - R_{ss}) * e^{-k_1 * t} + R_{ss} * e^{-k_2 * t} \quad \text{(Eq. 2)}$$

Observations to experimental data revealed that the decarboxylation reaction rate decreased heavily in the first few hours [4]. The process then became mild and tended to remain constant. To model both the heavy and mild decaying processes, the double exponential decay model (Eq. 2) was used as the objective function (Eq. 2), where R_0 represented the initial rate and R_{ss} corresponded to the rate during the relatively steady period. The independent variable of the function was time, t. The term e^(-k_i*t) described the decaying processes, with k_2 and k_1 representing the rate constants for fast and slow decays, respectively.

3.2 Similiarity between MFI and MOR, FER, FAU, BEA

Table 1 demonstrated that Brønsted acid sites were the primary category of acid sites for all catalysts examined in this study. As the silica content in MFI increased, the density of Brønsted and Lewis acid sites decreased. MOR and MFI 23:1 exhibited similar Brønsted site densities and Si:Al ratios, both around 1100 μmol/g/cat, with the silica content being at least twenty times higher than the alumina content. FER had a Si:Al ratio close to MFI 30:1, but its Brønsted site density was 154 μmol/g/cat lower.

Catalysts	Bet surface area (m^2/g)	Micropore area (m^2/g)	Pore diameter (A)	Pore volume (cm^3/g)	Brønsted sites (μmol/g/cat)	B:L ratio	Lewis sites (μmol/g/cat)
MFI Structure							
MFI 23:1	355.3769	241.0335	5.271	0.222169	1118	12.7	88
MFI 30:1	353.554	248.1221	5.408	0.272383	693	9.6	72
MFI 50:1	366.9874	228.6274	5.375	0.273374	358	5.3	68
MFI 80:1	385.712	305.3218	5.461	0.258955	327	6.5	50
MFI 200:1	354.0778	222.2481	5.513	0.210851	66	1.9	35
MFI 500:1	357.8402	228.6092	5.434	0.213315	29	1.2	24
Other Structure							
MOR (20:1)	395.0576	196.22	5.752	0.280731	1123	2.5	449
FAU (12:1)	669.156	567.1412	7.431	0.48272	633	2.2	288
BEA (25:1)	554.4564	352.299	6.534	0.828762	834	1.5	556
FER (20:1)	363.6704	322.9915	5.144	0.216602	539	1.2	449

Table 1 Physical and Acid Site information of MFI, MOR, FER, FAU, Beta [4]

Regarding the physical structures, MOR displayed similarities to the MFI family. Table 1 indicated that the surface area of the MFI family ranged from 353.5 m^2/g to 385.7 m^2/g, while MOR had a slightly higher surface area of 395 m^2/g. The pore diameter of MOR was slightly larger (0.24 Å/4.4%) compared to MFI 200:1 (5.51 Å, the highest). The pore volume of MOR fell within the range of MFI, ranging from 0.211 cm^3/g to 0.273 cm^3/g. The most significant difference was observed in the micropore area, where MOR exhibited a value of 196.2 m^2/g, 26 m^2/g lower than the smallest value in MFI (12%). FER also shared similarities in physical structure with the MFI family, with the first four categories in Table 1 being relatively close. However, FAU and BEA possessed unique properties, with significantly higher surface area, pore area, pore diameter, and pore volume compared to MFIs.

Given the similarities in physical structures, site categories, and Si:Al ratios, one might assume that the initial rate changes based on densities at various temperatures for MOR and its derivatives would follow similar pattern as that of the MFI family. A similar assumption could also be applied to FER and its derivatives. However, FAU and BEA may exhibit different behavior due to their distinctive properties.

During the MOR poisoning process, which involved immersing MOR zeolite in a $NaNO_3$ solution at 80°C for 12 hours, the H^+ ions in the Brønsted acid sites were exchanged with Na^+ cations present in the solution to lose acidity [25]. Regarding site and structure characterization, according to Rajamani, after undergoing the poisoning process, the Silica to Alumina ratio and the alumina not incorporated into the zeolite framework remained unchanged. The only variation observed was in the Sodium to Aluminum ratio and the distribution of acid sites. The former increased, while the latter decreased as the concentration of poisoning sodium nitrite increased [7].

3.3 Mass Normalized Initial Rate Trend over MFI Series

3.3.1 Initial Rate Trend over MFI using GVL as Reactant

The simulated initial rates of GVL decarboxylation over MFI zeolites, normalized by catalyst mass, were recorded in Table 2.

		Initial Rate (μmol/g/min)				
	Site Density μmol/g/cat	**158°C**	**178°C**	**198°C**	**218°C**	**238°C**
500:1	29	0.004263	0.0542	0.275		
200:1	66	0.0168	0.142	0.595		
80:1	327		0.541	2.64	14.3	54.9
50:1	358	0.101	0.671	3.70		
30:1	693	0.164	1.55	8.184236		
23:1	1118	0.142	1.744531	10.6	57.9	

Table 2 Numerical Data of Mass Normalized Initial Rate for GVL Decarboxylated over MFI Zeolites

The Koros and Nowark criterion was utilized to determine whether the catalytic reaction was kinetically controlled or influenced by intra-catalyst particle diffusion. This evaluation method was applicable to heterogeneous, metal catalysts and various reactor types such as batch, continuous stirred tank, and tubular plug flow reactors [24]. The criterion was based on the concept that the reaction rate was proportional to the concentration of active material (in this case, the Brønsted acid site density) on the catalyst surface [24].

One of the methods employed for Koros and Nowark criterion was plotting the logarithmically transformed mass-normalized reaction rates (simulated initial rate of decarboxylation) against the logarithm of the Brønsted site density. Linear regression analysis was employed to quantitatively

describe the relationship between the dependent and independent variables. The slope of the regression line played an important part in the evaluation, and it was related to the derivative between logarithmic diffusion efficiency and Thiele modulus. The Thiele modulus characterized the relationship between the reaction rate and diffusion rate [26]. The slope of the regression line was equal to 1 when the derivative reached 0. In this condition, the diffusion efficiency equal to one reached to its maximum. Therefore, a slope of 1 indicated that the reaction was kinetically controlled. Smaller derivatives led to smaller slopes of the regression line, indicating diffusion occurring in the reactor and inhibiting the catalyst's activity [24]. However, additional information and analysis were necessary to determine specific reasons causing diffusion limitations.

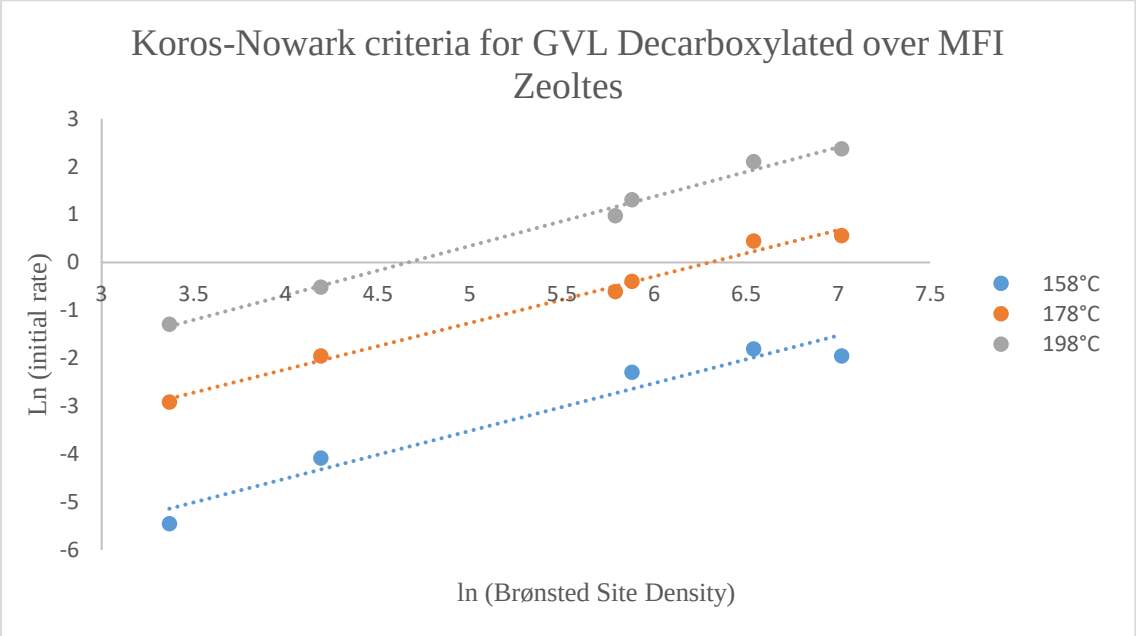

Figure 5 Koros-Nowark criteria for GVL Decarboxylation over MFI Zeolites at 158°C, 178°C and 198°C.

Figure 5 depicted the Koros-Nowark criteria for GVL decarboxylation over MFI zeolites at temperatures of 158°C, 178°C, and 198°C. The dependent variable represented the initial rate in logarithmic form with a base of the natural constant, while the independent variable was the

natural logarithm of the Brønsted site density. Data points under each temperature condition were evenly distributed on both sides of the linear regression line, and their coefficients of determination (R^2) were 0.95 (158°C), 0.99 (178°C) and 0.99 (198°C). This indicated the logarithm of initial rates exhibited a linear development along with the logarithm of Brønsted site density. The slopes of the linear relationships at temperatures ranged from 158°C to 198°C were 0.99, 0.97, and 1.03, respectively. These values were very close to 1, which can be interpreted as that GVL decarboxylation over MFI zeolites was kinetically controlled.

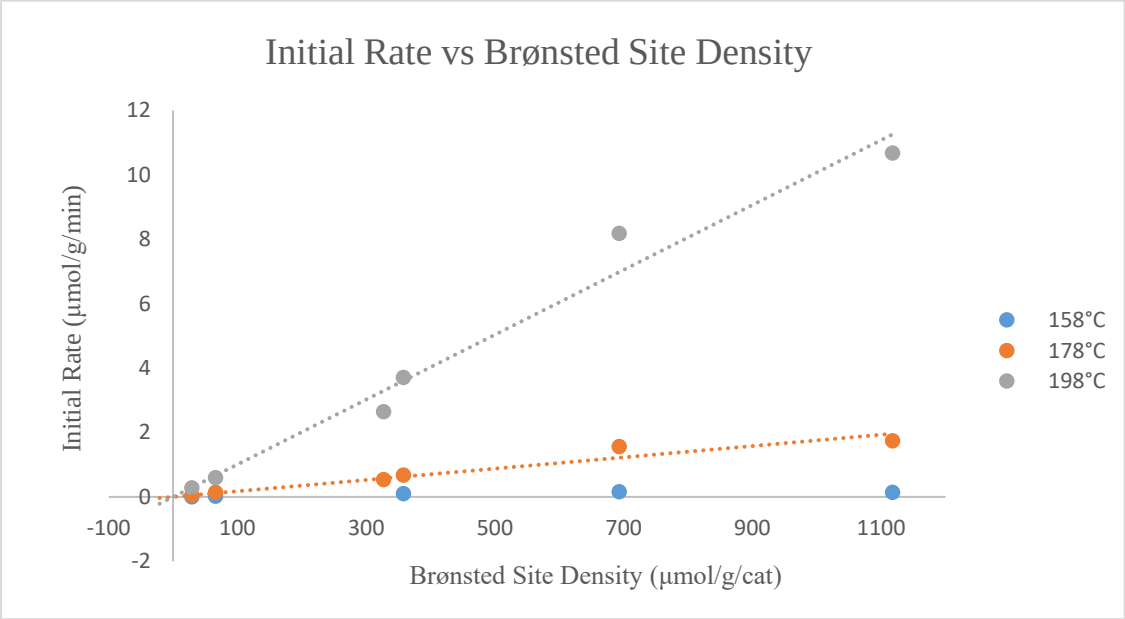

Figure 6 Simulated Mass-Normalized Initial Rate vs. Brønsted Site Density for GVL Decarboxylate over MFI zeolites at 198°C

In a previous study [4], a non-logarithmic plot of initial rate versus Brønsted site density was used to determine whether Brønsted acid sites were the only effective sites for decarboxylation. The linear trend line extrapolated through the origin point, where the initial rate was 0 μmol/g/min at the 0 μmol/g/cat Brønsted site density. This extrapolation indicated that no decarboxylation was

catalyzed in the absence of Brønsted acid sites, confirming that Brønsted acid sites were the only factors catalyzing the decarboxylation [4].

In this study, the relationship between the simulated mass-normalized initial rate and Brønsted site density of GVL decarboxylation over MFI zeolites at temperatures of 158°C, 178°C, and 198°C was plotted in Figure 6. The initial rate increased as the Brønsted site density increased at 178°C, and 198°C. The independent and dependent variables also exhibited good linearity, with even data point distribution and high coefficients of determination exceeding 0.95 at the temperature conditions. Extrapolating the trend line, they also passed through the origin point, supporting the conclusion mentioned in the previous study.

The slope of each line represented the average turnover frequency of the zeolites under different temperature conditions, calculated as the quotient of the initial rate divided by the site density. It was observed that as the temperature increased, the turnover frequency also increased.

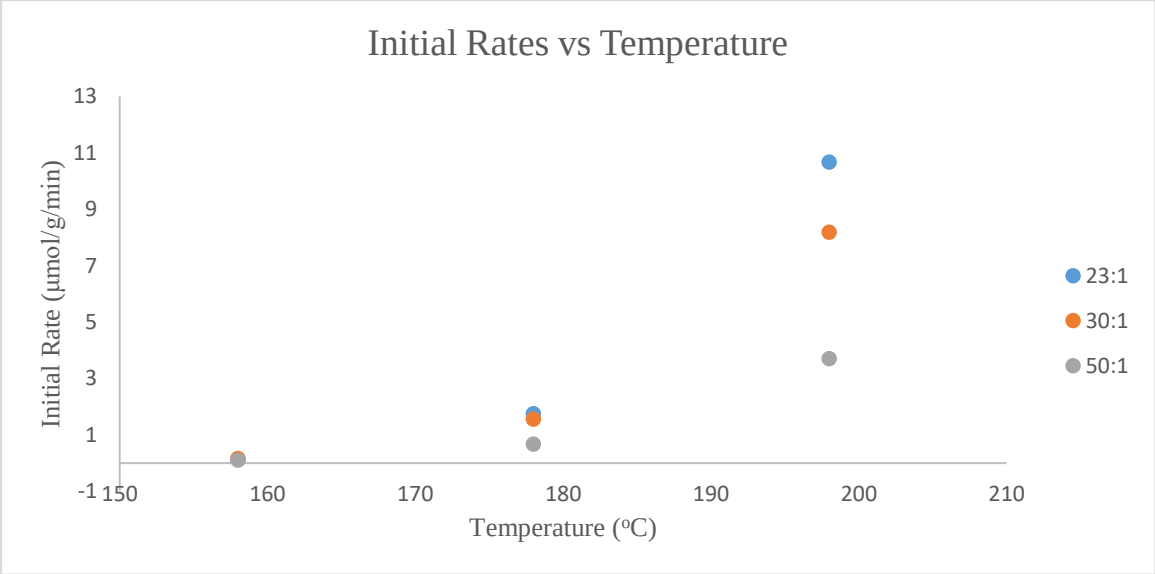

Figure 7(A) Mass Normalized Initial Rate vs. Temperature for GVL Decarboxylation over MFI Zeolite 23:1, 30:1, 50:1

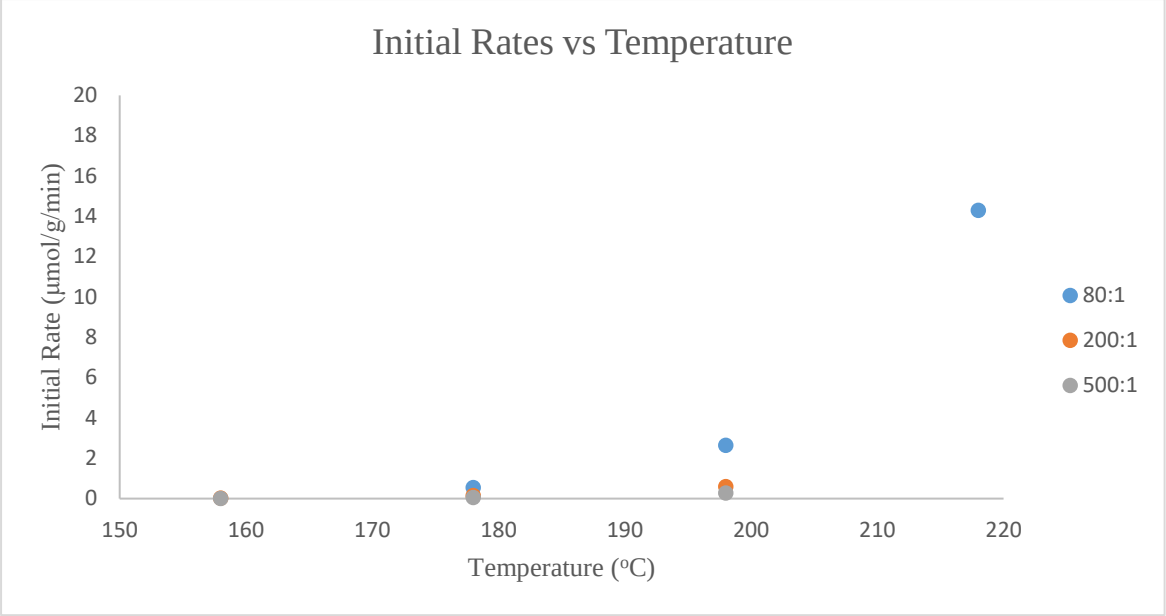

Figure 7(B) Mass Normalized Initial Rate vs. Temperature for GVL Decarboxylation over MFI Zeolite 80:1, 200:1, 500:1

Figure 7(A)(B) provided information on the change in mass-normalized initial rate with increasing temperature. Figure 7(A) displayed the initial rate data for MFI zeolites 23:1, 30:1, and 50:1, while Figure 7(B) showed data for reactions over MFI zeolites 80:1, 200:1, and 500:1.

It was evident that for MFI zeolites 23:1, 30:1, 50:1, and 80:1, the initial rates of decarboxylation increased as the temperature rose. These zeolites had relatively high Brønsted site densities ranging from 327 µmol/g/cat to 1118 µmol/g/cat. While it was difficult to differentiate from Figure 7(B) whether the initial rates over MFI 200:1 and MFI 500:1 followed a similar initial rate development trend, numerical data in Table 2 indicated that they also increased with temperature but by small amount of 0.27 µmol/g/min and 0.58 µmol/g/min. Additionally, for MFI 200:1 and 500:1, the standard deviations of its initial rates divided by their average at 158°C, 178°C, and 198°C were 1.2 for MFI 200:1 and 1.29 for MFI 500:1. Combining these information, we concluded that the initial rates changes of MFI 200:1 and MFI 500:1 were too small that they could be regarded as stabilized.

The trend of initial rate growth can be intuitively understood as follows: at higher temperatures, reactant molecules have a higher average velocity, making them more active and increasing their contact with the catalyst surface, which in turn enhances the reaction rate. From a different perspective, using the Arrhenius equation and the reaction rate expression, an increase in temperature causes the reaction constant k to increase. For a constant reactant concentration (partial pressure of GVL gas phase in helium), the reaction rate increases as the reaction constant k increases.

To avoid the influence of diffusion phenomena, zeolites catalyst loaded into the packed bed usually had small volume (weight) that can be loaded as a thin layer. MFI 200:1 and 500:1 had very low site density, so that their total site number in the bed were very small that even with the influence of high temperature, they could not generate noticeable large amount of butene product compared with those at lower temperature condition.

$$\ln(k) = \ln(A) - \frac{Ea}{k_b} * \frac{1}{T} \quad \textbf{Eq.3}$$

$$r = kC_{reactant} \quad \textbf{Eq.4}$$

3.3.2 Initial Rate Trend over MFI Using PEA as Reactant

Similar conclusions could be drawn when the reactant was changed to PEA. The normalized initial rates of decarboxylation over MFI zeolites are presented in Table 3 in the Appendix section.

Experimental data (GC area) of PEA decarboxylation over MFI were collected by different individuals, and they employed different methods to treat the GC noise signals. The GC noise signal refers to the detected butene areas when the reaction apparatus was running through the bypass channel for helium and reactant signal stabilization. One might choose to neglect the noise, while other might subtract the average noise butene area obtained from the reaction. Consequently, these methods could cause deviations in initial rates simulation, and further cause difficulties in applying the Koros-Nowark criteria to decarboxylation. In this research, to minimize these deviations among initial rates, experimental data were selected from a single source for reactions using a specific catalyst and reactant.

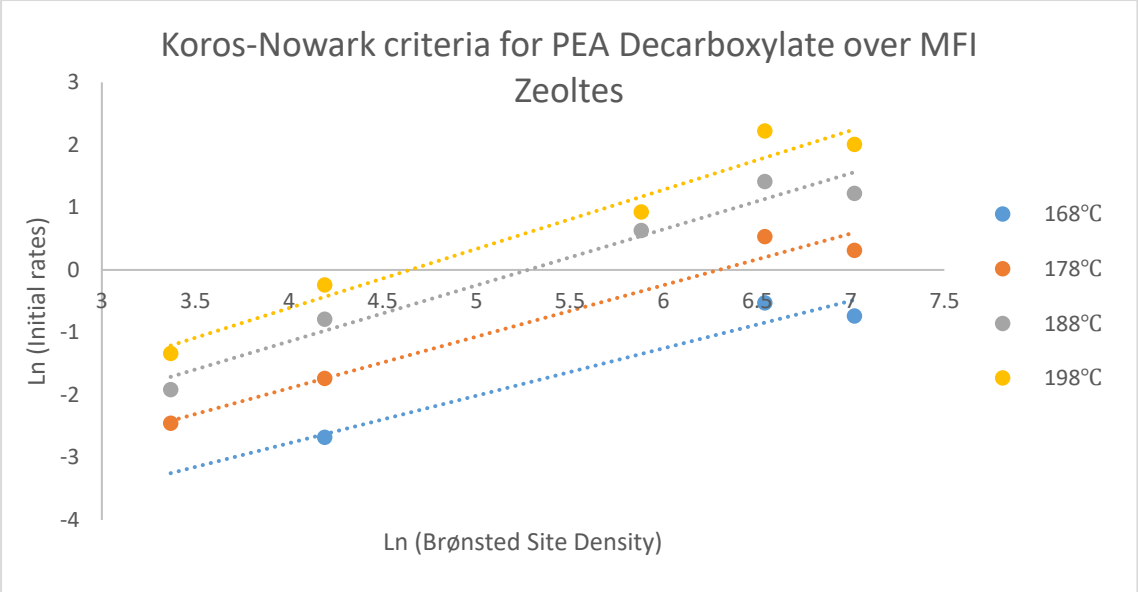

Figure 8(A) Koros-Nowark criteria for PEA Decarboxylation over MFI Zeolites from 168°C to 198°C

Figures 8(A) provided information about the Koros-Nowark criteria for the logarithmic mass-normalized initial rate versus Brønsted site density of PEA decarboxylation over MFI zeolites (500:1, 200:1, 50:1, 30:1, 23:1) from 168°C to 198°C. Based on visual inspections, the data points were evenly distributed along the trend line, and their determination coefficients were above 0.94, confirming their linearity. The slope of the Koros-Nowark criteria for each trend line were 0.76 (168°C), 0.82 (178°C), 0.89 (188°C), 0.94 (198°C), indicating the occurrence of diffusion phenomena. Additionally, an interesting observation was that the initial rates at MFI 23:1 decreased after MFI 30:1. This was consistent over the four temperature conditions. The observation will be explained in section 3.4.2 with PEA decarboxylation over MOR zeolites.

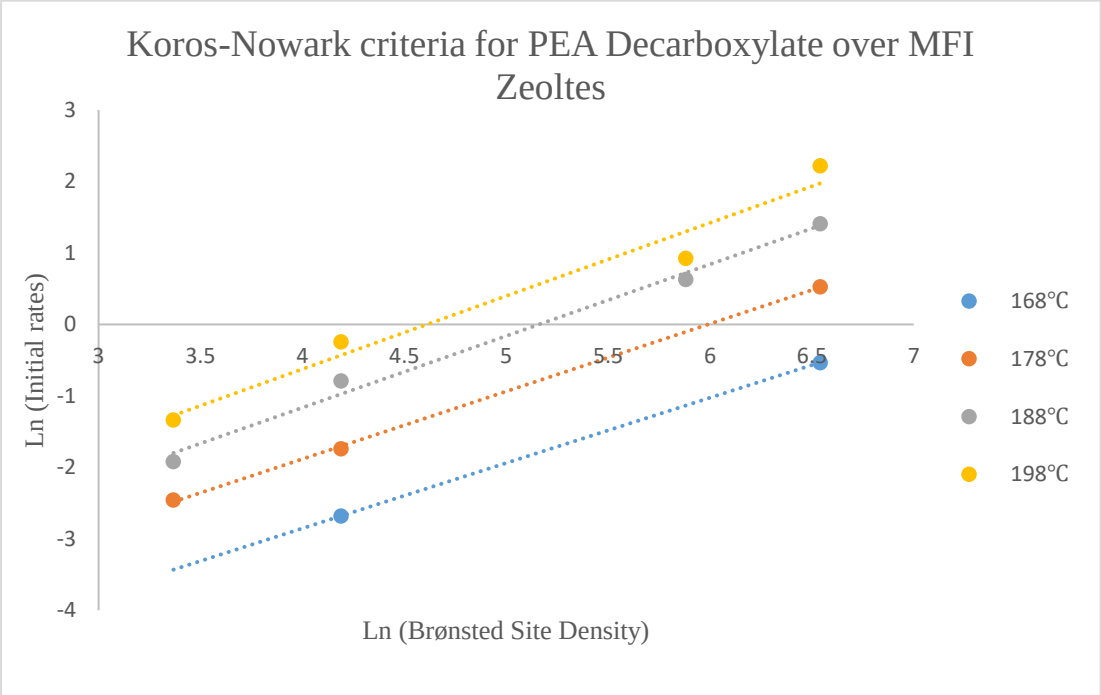

Figure 8(B) Koros-Nowark criteria for PEA Decarboxylation over MFI Zeolites without MFI 23:1

When the initial rates of MFI 23:1 were temporarily not considered, there was good linearity at all temperatures, as the data points are evenly distributed along the regression trend lines, and the

determination coefficients were 0.97 and above. The slope of the Koros-Nowark criteria becomes much closer to one. From 168°C to 198°C, the slopes were 0.91, 0.94, 1, and 1.02, respectively. Given the information above, the reactions over MFI 500:1, 200:1, 50:1, 30:1 from 168°C to 198°C could be evaluated as kinetically controlled, and reactions over MFI 23:1 has diffusion issues. Regarding the initial rate development with temperature, for the MFI zeolites mentioned above, the initial rates increase with temperature. This principle aligns with the application of Arrhenius equation (Eq.3) and the reaction rate expression (Eq.4) for GVL decarboxylation over MFI zeolites. Graphical trends are presented in Figure 9 in the appendix section.

In sections 3.3.1 and 3.3.2, GVL and PEA decarboxylation over MFI zeolites were evaluated using the Koros-Nowark criteria. The conclusions were that decarboxylations based on GVL over MFI 500:1 to 23:1 and PEA over 500:1 to 30:1 were kinetically controlled. For PEA decarboxylated over MFI 23:1, we considered diffusion phenomena existed. Additionally, the simulated initial rates for both reactants increased as the reaction temperature increased.

3.4 Mass Normalized Initial Rate Trend over MOR Series

3.4.1 Initial Rate Trend over MOR using GVL as Reactant

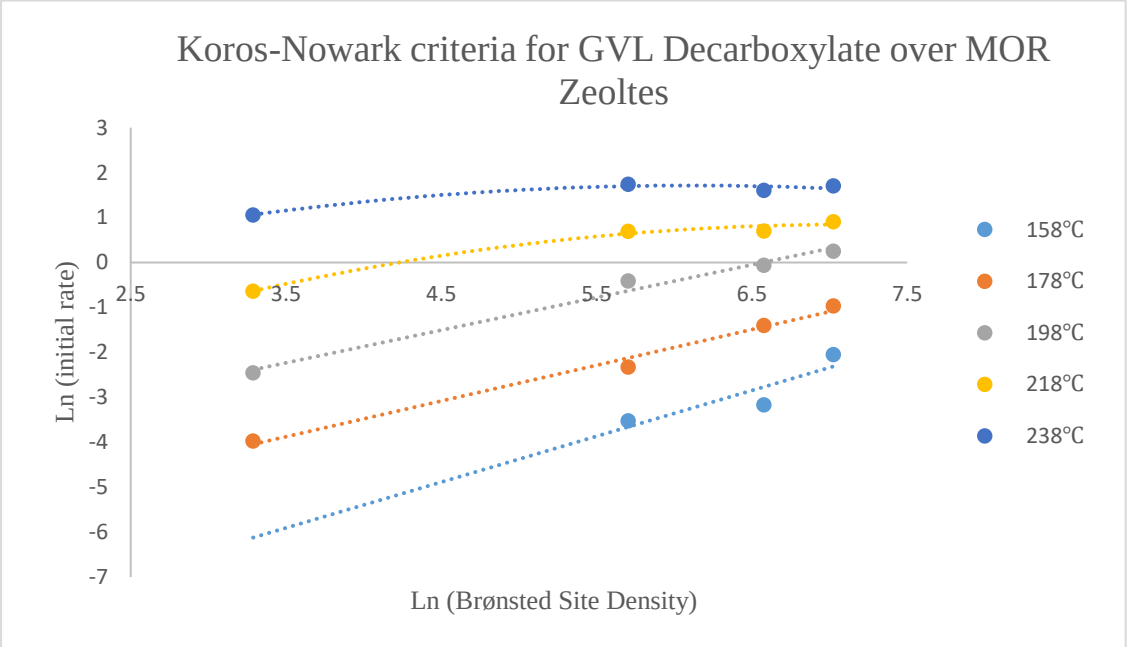

Figure 9 Koros-Nowark criteria for GVL Decarboxylation over MOR Zeolites at 158°C, 178°C, 198°C, 218°C and 238°C.

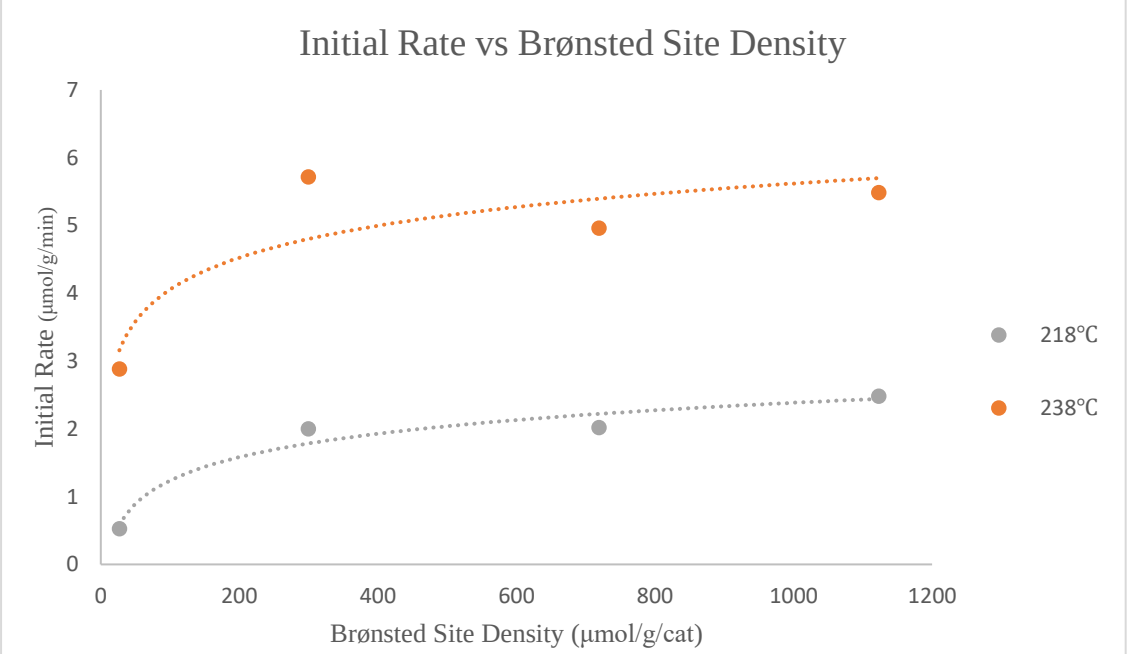

Figure 10 Simulated Mass-Normalized Initial Rate vs. Brønsted Site Density for GVL Decarboxylate over MOR zeolites at 218°C and 238°C

Figure 9 shows the Koros-Nowark criteria for GVL decarboxylation over MOR zeolites from temperatures 158°C to 238°C. Similar to the pattern observed for GVL decarboxylation over MFI zeolites, from 158°C to 198°C, the logarithmic initial rates also increase linearly with the logarithmic Brønsted site density. A noticeable observation at 158°C was the slope of the trend line was 1.02, indicating a kinetic control over the reaction. As the temperature increases, the slope decreased to 0.79 at 178°C and 0.72 at 198°C indicating a gradual significant diffusion development with temperature increase. This phenomenon could be explained using the mathematical expression of Peclet number (Pe) and the mass diffusion coefficient. The Peclet number relates the convection and diffusion phenomena, where a higher Pe number indicates convection control which could be simply understood as kinetic control in the case of decarboxylation. A lower Pe number suggests diffusion dominance. The Pe was calculated by multiplying the flow velocity (v) and characteristic length (L) and dividing it by the mass diffusion coefficient (D) (Eq. 5). The mass diffusion coefficient was calculated using equation 6, where D_0 was the maximal diffusion coefficient, Ea was the activation energy for diffusion, and R was the universal gas constant. As the temperature increased, assuming activation energy and the maximal diffusion coefficient remained constant, the mass diffusion coefficient also increased. This led to a decrease in the Peclet number, indicating an increasing diffusion influence within the packed bed system.

$$Pe = \frac{v*L}{D} \quad \text{Eq. 5}$$

$$D = D_0 * e^{\frac{Ea}{R*T}} \quad \text{Eq.6}$$

At 218°C and 238°C, the logarithmic initial rates and logarithmic Brønsted site density no longer followed a linear trend. Figure 10 presented the plot of simulated initial rate versus Brønsted site density at reaction temperatures of 218°C and 238°C. It was observed that the reaction rates initially showed an increase, and when the site density reaches 299 μmol/g/cat and above, they seemed to stabilize. For initial rates at densities of 299 μmol/g/cat, 719 μmol/g/cat, and 1123 μmol/g/cat, the linear trend lines at the two temperatures had slopes of 0.0006 (218°C) and 0.0003 (238°C), the standard deviations over the average of 12.5% for 218°C and 7.2% for 238°C across the density change of nearly 1000 μmol/g/cat. These information suggested that there were nearly no changes in initial rates for 0.1M NaNO3 poisoned MOR, 0.01M NaNO3 poisoned MOR and non-poisoned MOR at 218°C and 238°C, and the initial rates stabilize at 2.16 μmol/g/min and 5.38 μmol/g/min respectively.

In Section 3.2, structural information highlighted that although MOR zeolites had higher surface area, pore diameter, and pore volume compared to MFI zeolites, their micropore area was smaller. The micropore area was relevant to the accessibility of reactants to active sites inside the pores, and could also impose limits on the diffusion of products out of the pores. Additionally, Wang's research [18] indicated that MOR zeolites have two types of channels: 12-member and 8-member ring channels. The 8-member ring channels had a complex structure similar to enzymes [7], which could further contribute to diffusion difficulties for reactant diffusing into the channel and the product diffusing out. At higher temperature conditions, both the reactant average velocity and the reaction rates increased. Also, catalysts with more Brønsted active sites generated more butene products. When site density reached 299 μmol/g/cat, and reaction temperature reached 218 °C, the both product and reactant diffusion reached to their maximum rates. Hence, the observed butene production decarboxylation rate remained constant.

Consequently, in experiments, at 158, the initial rate showed behavior characteristic of kinetic control, but as the temperature increases, diffusion has become more obvious. Finally, when the temperature reaches 218°C and above, the initial rate at high Brønsted site densities remains similar to the rates at lower site densities (299 μmol/g/cat).

Information about initial rates at different temperatures for GVL decarboxylated over MOR zeolites can be found in Table 4 in the appendix.

3.4.2 Initial Rate Trend over MOR using PEA as Reactant

		Initial Rate (μmol/g/min)				
	Site Density μmol/g/cat	**158°C**	**178°C**	**198°C**	**218°C**	**238°C**
1M	26.8	0.044	0.13	0.30	1.2	5.2
0.1M	299.65	0.067	0.36	1.4	3.9	5.9
0.01M	719	0.10	0.29	1.2	3.1	5.8
MOR	1123	0.067	0.18	0.45	1.09	2.8

Table 5 Numerical Data of Mass Normalized Initial Rate for PEA Decarboxylated over MOR Zeolites

When applying the Koros-Nowark method to the initial rates of PEA decarboxylation over MOR zeolites, data points of logarithm initial rates seemed to be relatively stabilized along the logarithm Brønsted site density. However, an obvious decrease was observed at the density of non-poisoned MOR (1123 μmol/g/cat) at all temperature conditions (Figure 11). This was similar to the situation of PEA decarboxylation over MFI zeolites (Figure 8A).

By temporarily not considering the data points at 1123 μmol/g/cat (Figure 12), one could presume that the initial rate of decarboxylation stabilized at 238°C condition. From 178°C to 198°C, the initial rates first experienced a growth from 26.8 μmol/g/cat (1M NaNO3 poisoned MOR) to 299 μmol/g/cat. From densities of 299 μmol/g/cat to 719 μmol/g/cat, which corresponded to 0.1M NaNO3 poisoned MOR and 0.01M NaNO3 poisoned MOR, logarithm initial rates became stabilized.

Figure 13 and Figure 14 provided information on the simulated initial rate changes along with density increase. From visual observation, the stabilization of initial rates across the densities did not seem to be obvious. To quantitatively evaluate the stability of the initial rates at 178°C, 198°C, 218°C, and 238°C, numerical values of initial rates in Table 5 were considered.

The linear regression trend line through the data points of 0.1M NaNO3 poisoned MOR and 0.01M NaNO3 poisoned MOR at each temperature condition had the absolute slope of 0.260, 0.244, and 0.241 from 178°C to 218°C across the site density range of 319 μmol/g/cat. The standard deviations of initial rates divided by their averages at each temperature were 0.16, 0.15, and 0.15, respectively. Additionally, the absolute rate changes at these temperatures were very small as 0.07, 0.28 and 0.74 μmol/g/min for 178°C, 198°C and 218°C. Given the information above, we considered the simulated initial rate changes between 0.1M NaNO3 poisoned MOR and 0.01M $NaNO_3$ poisoned MOR at 178°C, 198°C, and 218°C were too small to be regarded as reaching stabilization. As the standard deviation over the average was small (0.06) for all $NaNO_3$ poisoned MOR zeolites at 238°C, it was also considered that the initial rates of these catalysts has reached stabilization.

The stabilization in initial rates of PEA decarboxylated over MOR zeolites from 178°C to 198°C was similar to that observed for GVL decarboxylated over the MOR zeolites from 218°C to 238°C. They were considered sharing the same reasons as small pore area and complex channel structure caused diffusion limitation to both reactant and products. Hence, initial rates at high Brønsted acid site densities were limited to the values close to those at lower site densities.

The drops in initial rate at the density of non-poisoned MOR (1123 μmol/g/cat) at all temperature conditions (Figure 11) were similar to the observations for PEA decarboxylated over MFI zeolites. The observations seemed strange because the Brønsted acid site was the only effective site for the decarboxylation reaction (section 3.3.1), so reactions over higher site density should result in a higher initial rate. If diffusion limitation existed in the system, the corresponding initial rates should remain relatively the same as that at lower site densities. Other factors should have been prohibiting the reaction of PEA decarboxylation over MFI and MOR zeolites.

The PEA molecule had a chain structure. When the molecule decarboxylated over the Brønsted acid site, the carboxyl group approached the site and received (H^+) from the site to generate a chain structure intermediate. Later, the intermediate lost the carboxyl group to generate CO_2 and butene.[11] The chain consisted of 4 carbon-carbon single bonds with a length of 153.5 pm [28] and 1 carbon-oxygen single bond with a length of 136 pm [28], resulting in an approximate length of 750 pm (0.75 nm), because of the angles between chemical bonds. According to Wang and Zhang [18], the channel dimensions of MOR was 0.67 nm × 0.7 nm for the 12-membered ring channel, and 0.26 nm × 0.57 nm for the 8-membered ring channel. Hence, the intermediate length was at the same order of magnitude as the dimensions of the MOR channels. MOR, compared to 0.01M NaNO3 poisoned MOR, had nearly twice the Brønsted site density of 1123 μmol/g/cat. With PEA molecules spiking in the channels, diffusion of free PEA molecules to vacant sites in the deeper locations of the channels became more difficult, same for butene molecules diffusing out of the catalyst. This significantly hindered the decarboxylation rate. Similarly, for PEA decarboxylation rate drop over MFI 23:1, the zeolite had a Brønsted site density close to non-poisoned MOR, both at a level of 1100 μmol/g/cat. The channel dimensions of the MFI zeolites was 0.51 nm × 0.55 nm and 0.53 nm × 0.56 nm [29] which were even smaller than that of MOR, so similarly, crowdy channels of MFI 23:1 caused diffusion limitations to PEA and butene, and observed was the reaction rate drop over the catalyst.

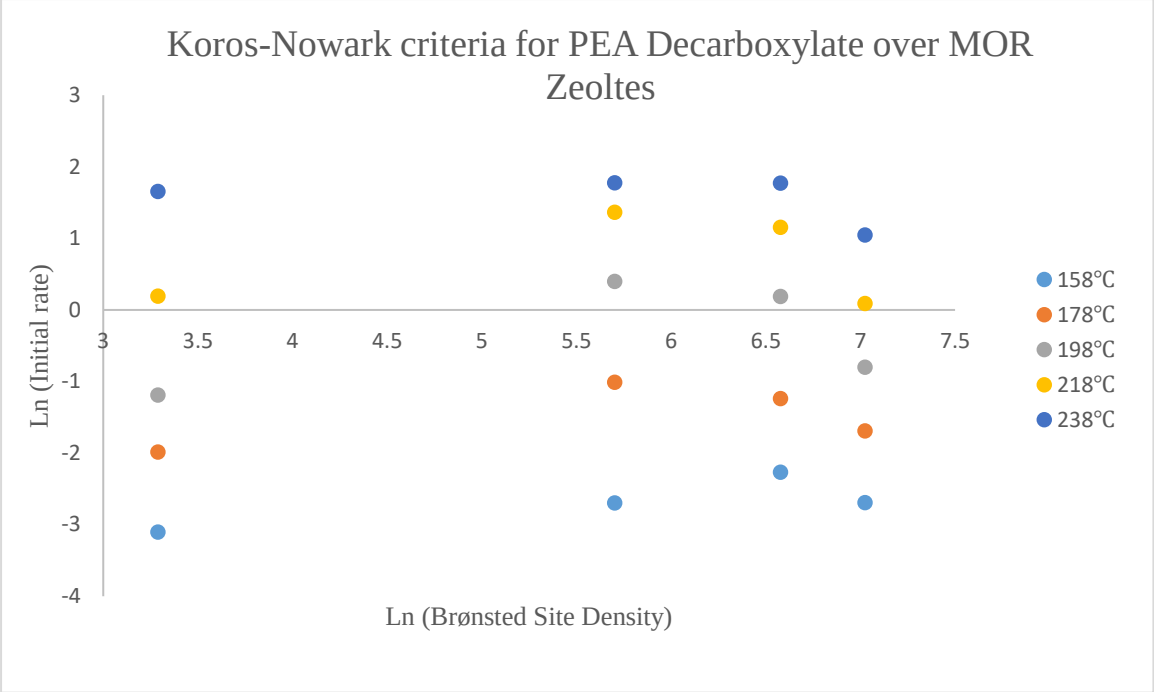

Figure 11 Koros-Nowark criteria for PEA Decarboxylation over MOR Zeolites at 158°C, 178°C, 198°C, 218°C and 238°C.

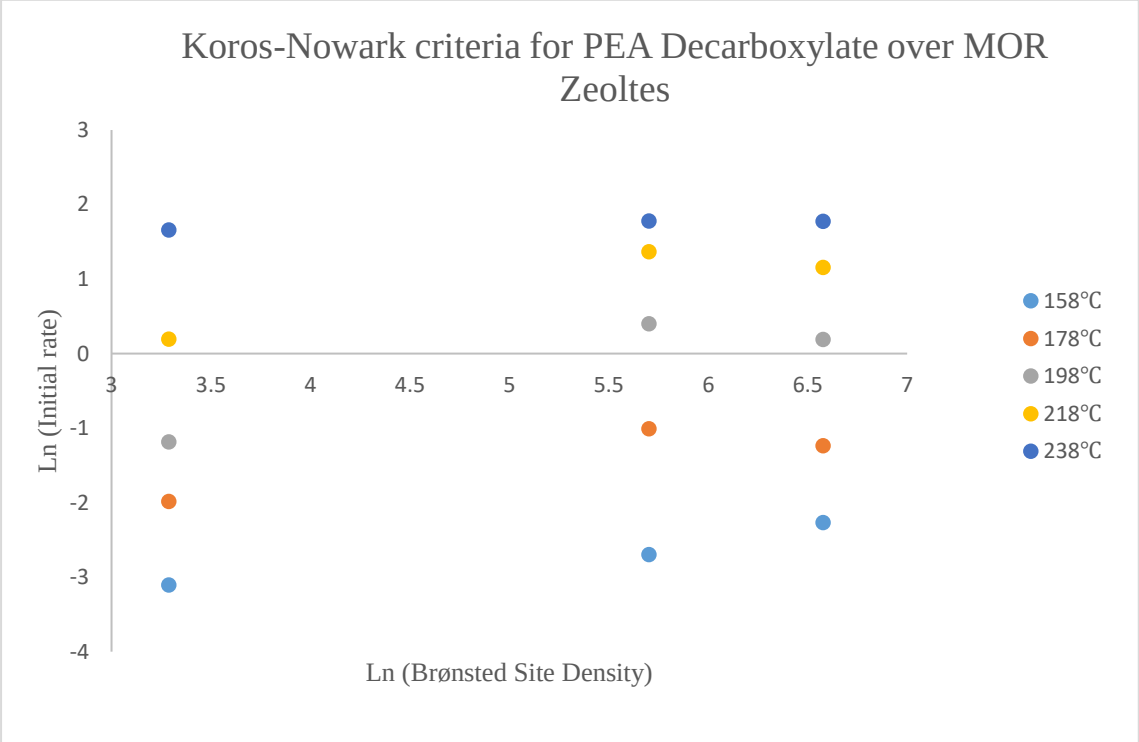

Figure 12 Koros-Nowark criteria for PEA Decarboxylation over poisoned MOR Zeolites from 158°C to 238°C.

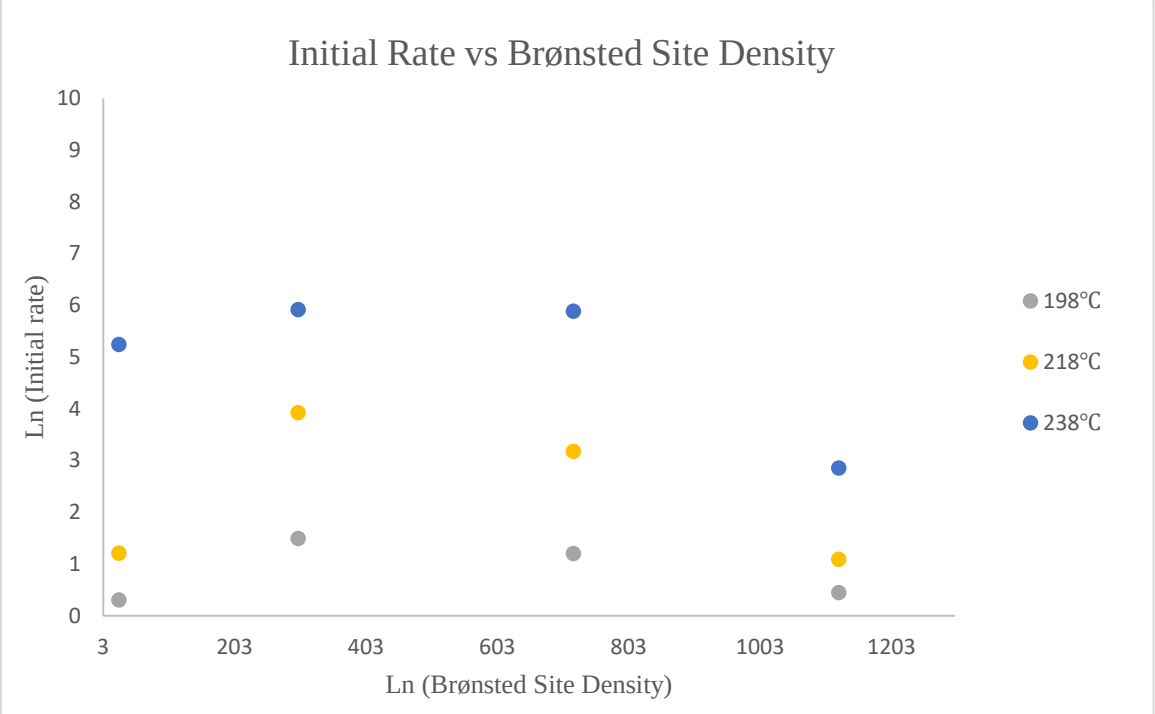

Figure 13 Simulated Mass-Normalized Initial Rate vs. Brønsted Site Density for PEA Decarboxylate over MOR zeolites at 198°C, 218°C and 238°C

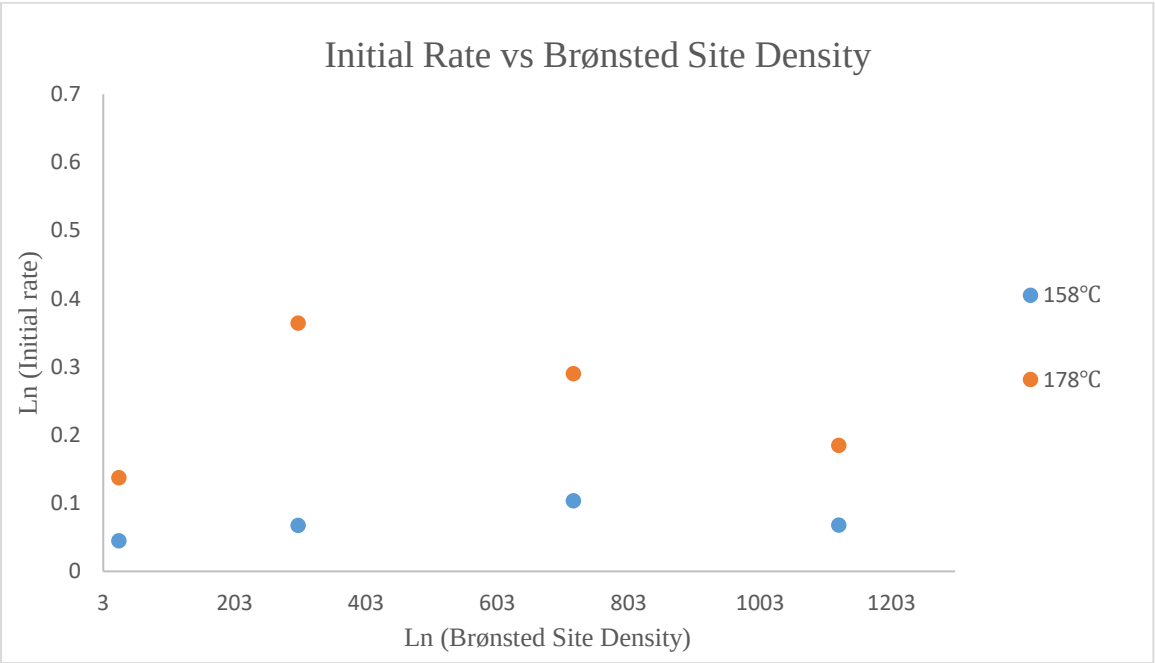

Figure 14 Simulated Mass-Normalized Initial Rate vs. Brønsted Site Density for PEA Decarboxylate over MOR zeolites at 158°C and 178°C

4. Conclusion

This study investigated the decarboxylation reactions of GVL and PEA over MOR and MFI zeolites. The results revealed the influence of catalyst properties, such as Brønsted site density, pore and channel structures, on the diffusion phenomena and reaction rate change.

For GVL decarboxylation over MFI zeolites, the reactions were found to be kinetically controlled based on the Koros-Nowark criteria. However, when decarboxylating GVL over MOR zeolites series, stabilizations of initial rates were observed. The small pore areas and complex channel structures of MOR zeolites hindered the diffusion of reactants into the catalyst and products out of the catalyst, and further limiting the reaction rate. Consequently, the observed reaction rates remained constant at higher Brønsted site densities.

Similar diffusion limitations and initial rate drops were observed for PEA decarboxylation over MFI 23:1 and non-poisoned MOR zeolites. Reasons causing the rate drop was the high Brønsted site density of MFI 23:1 and non-poisoned MOR and the long-chain structure of the PEA molecules. As PEA molecules spiked in the catalyst channels during reaction. reactant and product diffusions were limited, and led to a reduction in the initial reaction rate.

5. Future work

5.1 Brønsted site density of FER, FAU, BEA

To investigate whether diffusion was limiting the initial rate capabilities of FER, FAU, and BEA, they were treated with 0.1M NaNO3. However, the Brønsted site densities of these derivatives were not available due to equipment issues. As a result, the site densities of these derivatives were estimated based on the ratio between the site densities of poisoned and non-poisoned MOR. The mass of the poisoned FER, FAU, and BEA loaded in the packed bed were calculated based on estimated densities. Due to these inaccuracies, simulated initial rates constained many uncertainties. To improve the accuracy of future work, the Brønsted site densities of FER, FAU, and BEA derivatives need to be determined.

5.2 Alternative in Initial Rate Simulation Using Julia Language

The primary concept of simulating initial rate in Julia is also the Error Sum of Squares method (Eq. 1), which is stored in the LeastSquaresOptim package. The algorithm requires an objective function that describes the rate decay and parameters in the function as inputs [22]. In addition to the two-phase model, which may be too general in describing the decay trend, a new and creative idea has been attempted by using an objective function that simulates the decaying and increasing progress of reactants and products to steady states. This objective function is based on a system differential algebraic equations of mass balance over a packed bed reactor and catalyst surface to accurately describe the flow coming out of the reactor. The code involves solving and transient continuous stirring tank reactor (which provides initial conditions for the packed bed reactor solver), the packed bed reactor model, and adjusting parameters to search for the least SSE.

During program testing, the code failed to calculate the result [21]. Both mathematical knowledge and reactor design expertise are required to optimize the code.

6. Appendix

	Initial Rate (µmol/g/min)						
	Site Density µmol/g/min	158°C	168°C	178°C	188°C	198°C	218°C
500:1	29			0.0541	0.122179	0.257996	0.823537
200:1	66		0.051547	0.105792	0.403785	0.785029	
50:1	358			0.201652	1.876918	2.522363	
30:1	693		0.58777	1.698133	3.891073	8.221906	50.10512
23:1	1118	0.167855	0.777517	1.767063	4.696207	10.41266	

Table 3 Numerical Data of Mass Normalized Initial Rate for PEA Decarboxylated over MFI Zeolites

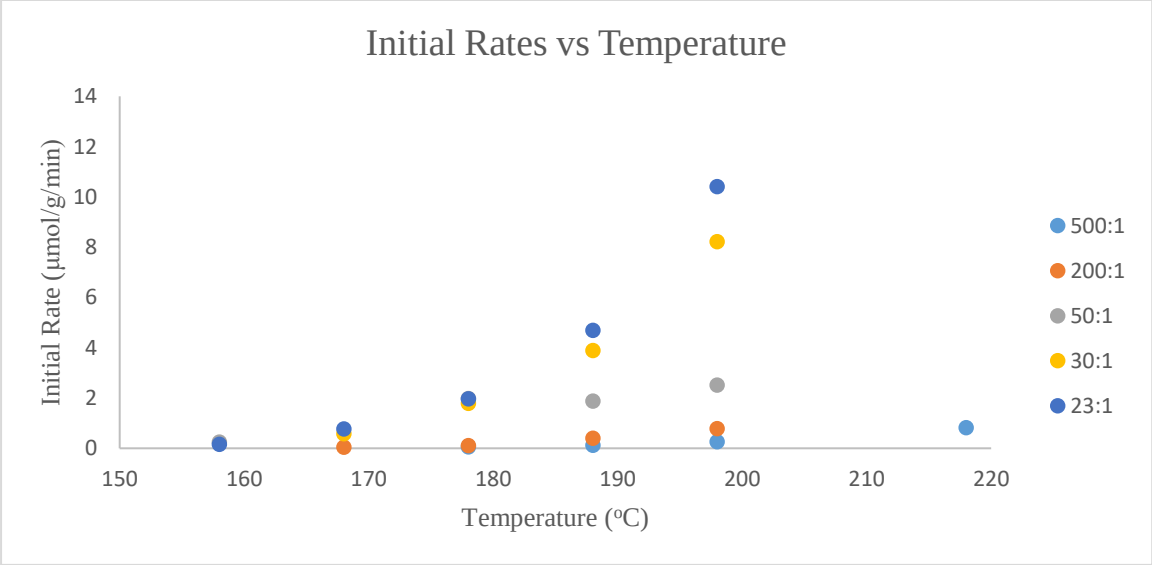

Figure 9 Mass Normalized Initial Rate vs. Temperature for PEA Decarboxylation over MFI Zeolite

	Initial Rate (μmol/g/min)					
	Site Density μmol/g/cat	**158°C**	**178°C**	**198°C**	**218°C**	**238°C**
1M	26.8		0.018766	0.085861	0.52701	2.885122
0.1M	299.65	0.029451	0.097427	0.661159	2.001238	5.719685
0.01M	719	0.042163	0.245574	0.94138	2.017966	4.961605
MOR	1123	0.13891	0.38	1.282802	2.4808	5.486676

Table 4 Numerical Data of Mass Normalized Initial Rate for GVL Decarboxylated over MOR Zeolites

7. Reference

1. B. Kamm, M. Gerhardt, G. Dautzenberg. Catalytic Processes of Lignocellulosic Feedstock Conversion for Production of Furfural, Levulinic Acid, and Formic Acid-Based Fuel Components. In: New and Future Developments in Catalysis [Internet]. Elsevier B.V.; 2013 [cited 2023 May 1]. p. 9–113. Available from: https://www.sciencedirect.com/science/article/pii/B9780444538789000059?via%3Dihub

2. Bond JQ, Alonso DM, Wang D, West RM, Dumesic JA. Integrated Catalytic Conversion of γ-Valerolactone to Liquid Alkenes for Transportation Fuels. Science. 2010 Feb 26;327(5969):1110–4.

3. Bond JQ, Alonso D, Ryan, Dumesic JA. γ-Valerolactone Ring-Opening and Decarboxylation over SiO_2/Al_2O_3 in the Presence of Water. Langmuir. 2010 Jun 1;26(21):16291–8.

4. Huang X. An examination of γ-valerolactone ring opening and decarboxylation in multiphase system and over various solid acid catalysts [pdf]. Bond J, editor. [Syracuse University]; 2021. p. 103–25.

5. Bond JQ, Wang D, Alonso DM, Dumesic JA. Interconversion between γ-valerolactone and pentenoic acid combined with decarboxylation to form butene over silica/alumina. Journal of Catalysis. 2011 Jul;281(2):290–9.

6. Huber GW, Dale BE. Grassoline at the Pump. Scientific American. 2009 Jul;301(1):52–9.

7. Gounder R, Iglesia E. Catalytic Consequences of Spatial Constraints and Acid Site Location for Monomolecular Alkane Activation on Zeolites. Journal of the American Chemical Society. 2009 Jan 15;131(5):1958–71.

8. Kellicutt AB, Salary R, Abdelrahman OA, Bond JQ. An examination of the intrinsic activity and stability of various solid acids during the catalytic decarboxylation of γ-valerolactone. Catalysis Science & Technology. 2014;4(8):2267.

9. Huang X. An examination of γ-valerolactone ring opening and decarboxylation in multiphase system and over various solid acid catalysts [pdf]. Bond J, editor. [Syracuse University]; 2021. p. 9–14.

10. Pierre Gallezot. Metal Catalysts for the Conversion of Biomass to Chemicals. In: New and Future Developments in Catalysis [Internet]. Elsevier B.V.; 2013 [cited 2023 May 1]. p. 9–113. Available from: https://www.sciencedirect.com/science/article/pii/B9780444538789000059?via%3Dihub

11. Bond JQ, Jungong CS, Chatzidimitriou A. Microkinetic analysis of ring opening and decarboxylation of γ-valerolactone over silica alumina. Journal of Catalysis. 2016 Dec;344:640–56.

12. Horváth IT, Mehdi H, Fábos V, Boda L, Mika LT. γ-Valerolactone—a sustainable liquid for energy and carbon-based chemicals. Green Chem. 2008;10(2):238–42.

13. Manzer LE. Catalytic synthesis of α-methylene-γ-valerolactone: a biomass-derived acrylic monomer. Applied Catalysis A: General. 2004 Sep;272(1-2):249–56.

14. Mehdi H, Fábos V, Tuba R, Bodor A, Mika LT, Horváth IT. Integration of Homogeneous and Heterogeneous Catalytic Processes for a Multi-step Conversion of Biomass: From Sucrose to Levulinic Acid, γ-Valerolactone, 1,4-Pentanediol, 2-Methyl-tetrahydrofuran, and Alkanes. Topics in Catalysis. 2008 Apr 5;48(1-4):49–54.

15. Decarboxylation Reaction | Correlation between Carboxylation & Decarboxylation [Internet]. BYJUS. [cited 2023 May 6]. Available from: https://byjus.com/chemistry/decarboxylation-reaction/#:~:text=Decarboxylation%20reaction%20is%20defined%20as%20a%20chemical%20reaction

16. GEOLOGYSCIENCE. Zeolite Mineral Groups |Properties, Occurrence, Uses» Geology Science [Internet]. Geology Science. 2019 [cited 2023 May 6]. Available from: https://geologyscience.com/minerals/zeolite/

17. Jae Hyun Kim. Decoupling of Economy from Fossil Fuels. 2017 Dec 17 [cited 2023 May 8]; Available from: http://large.stanford.edu/courses/2017/ph240/kim-j2/

18. Wang Y, Zhang Y, Liu W, Yu Q, Liu Z, Xu S, et al. An efficient synthesis strategy for MOR zeolite. Microporous and Mesoporous Materials. 2022 Dec;346:112282.

19. Kevan L. Microporous Materials: Zeolites, Clays, and Aluminophosphates. Encyclopedia of Physical Science and Technology. 2003;755–64.

20. Bond J. Solutions for Transient Reactors-Simple_2. 2023.

21. Bond J. GVL_SB.jl. 2023.

22. Bond J. Julia supplement - supplement 14 -15. 2023.

23. What is sintering in relation to catalyst deactivation and how can it be avoided? (PTQ Q&A) [Internet]. www.digitalrefining.com. [cited 2023 May 9]. Available from: https://www.digitalrefining.com/article/1002524/what-is-sintering-in-relation-to-catalyst-deactivation-and-how-can-it-be-avoided-ptq-q-and-#:~:text=Sintering%20is%20broadly%20termed%20as%20a%20physical%20and%2For

24. Madon RJ, Boudart M. Experimental criterion for the absence of artifacts in the measurement of rates of heterogeneous catalytic reactions. Industrial & Engineering Chemistry Fundamentals. 1982 Nov;21(4):438–47.

25. Bhan A, Allian AD, Sunley GJ, Law DJ, Iglesia E. Specificity of Sites within Eight-Membered Ring Zeolite Channels for Carbonylation of Methyls to Acetyls. Journal of the American Chemical Society. 2007 Mar 31;129(16):4919–24.

26. Ruthven DM. Studies in surface science and catalysis. Jiří Čejka, editor. Vol. 168. Amsterdam: Elsevier; 2007.

27. Rapp BE. Microfluidics : Modeling, Mechanics, and Mathematics. Amsterdam Elsevier; 2017.

28. Bruno TJ, Lide DR, Rumble JR. CRC handbook of chemistry and physics : a ready-reference book ofchemical and physical data. Boca Raton: Crc Press; 2018.

29. MFI: Type Material [Internet]. asia.iza-structure.org. [cited 2023 May 25]. Available from: https://asia.iza-structure.org/IZA-SC/material_tm.php?STC=MFI

Weixuan Huang

Address: Apt.204,121 Lafayette Rd, Syracuse, NY, USA13205**/ Tel.:**(1)3159139775**/Email:** whuang42@syr.edu

Education

Syracuse University, United States of America (M.S.) ……..**2020–2022**

The University of Edinburgh, United Kingdom (B.S.) …….. ….**2015-2017**

Liaoning Shi Hua University, China (B.S.)……**2013-2015**

Research Experience:

Syracuse University, USA……1/2020 – 6/2022

- Participate in project *Resolving Impacts of Acidity and Morphology on Decarboxylation over Solid Acid Catalyst*:
    - Assembling and operating gas phase reaction system using differential packed bed reactors
    - Gas chromatography
    - Temperature programmed desorption of amines to determine Bronsted Acid site densities
    - Kinetic date analysis
- Catalyst surface characterization by modified steady state isotopic-transient kinetics analysis
    - Using transient methods to study the oxidation of ketones on Vo_x/gamma Al_2O_3
    - Reactor operation, data collection, gas chromatography

Infinitus Company Ltd, Guangzhou China……10/2018 – 12/2018

- Interned in the Department of Self-care and Household Cleaning.
- Product design in various groups (Marketing, Facial Products, Daily Products, Overseas)
- Literature research in microfluidics, microneedles, biological environment of scalp and dandruff, and experimental models for allergic rhinitis
- Participate in market report study and department meetings

The University of Edinburgh, UK……..2015-2017

- Group design of *R32 Manufacture for Mexichem company* designing two distillation towers.
- Group dissertation of *Nanotechnology in Tissue Engineering with United Healthcare*.
- Thesis project of *Advances in Equations of States of Fluids*
- Personal design of heat exchanger

Awards:

- Certification for Completing Python Summer Course by Syracuse University School of Engineering and Computer Science……..**7/2020**
- 1st in British University College Sport 3A with Edinburgh University Men's Basketball Third Team ……..**2016-2017**
- Multiple awards in speech competitions in LiaoNingShiHua University.....……**2013-2014**

Skills

- Liquid and gas phase flow reactor operation
- Transient reactor operation
- System maintenance and trouble shooting
- Temperature-programmed desorptions for active site titration

- Computer skills: MatLab, Python and Auto CAD, UniSim, Microsoft Office.

Additional Experience:

- AICHE 2020-2021 annual conference in Boston……**11/2021**
- Volunteer at Edinburgh University Open days……..**2015-2017**
- Volunteered at Guangdong 999 Brain Hospital taking care of patients ……..……**2014**